International Journal of Environmental Science and Technology (2026) 23:191
https://doi.org/10.1007/s13762-025-06984-3

ORIGINAL PAPER

Photocatalytic removal of acetamiprid using ZnO and TiO_2-doped ZnO: kinetic and degradation pathway analysis

E. S. Eroğlu[1] · M. B. Akın[2] · G. D. Değermenci[1]

Received: 4 August 2025 / Revised: 21 November 2025 / Accepted: 3 December 2025 / Published online: 29 December 2025

Abstract

In this study, the photocatalytic removal of acetamiprid (ACE) was investigated using ZnO and TiO_2-doped ZnO photocatalysts. The effects of different light sources (simulated solar light, UV-A, and UV-C) were evaluated, with the highest performance obtained under UV-C light. Parameters affecting the photocatalytic process, such as pH, catalyst amount, and initial concentration, were examined, and the optimum catalyst amount was determined to be 1 g/L. Kinetic analyses showed that the degradation rate of ACE followed a pseudo-first-order kinetic model. HPLC analyses revealed that ACE was completely degraded (100% removal) after 120 min of reaction; however, UV spectrophotometer analyses identified a removal efficiency of 79% for ZnO and 71% for TiO_2-doped ZnO, due to the presence of intermediate products. LC–MS/MS analyses identified the intermediate products formed during the photocatalytic degradation process of ACE, confirming effective mineralization. The findings demonstrate that ZnO and TiO_2-doped ZnO are effective photocatalysts for the removal of ACE and hold significant potential for environmentally sustainable treatment technologies.

Editorial responsibility: Samareh Mirkia.

✉ G. D. Değermenci
gdegermenci@kastamonu.edu.tr; gokcendidar@gmail.com

[1] Department of Environmental Engineering, Faculty of Architecture and Engineering, Kastamonu University, Kastamonu 37150, Türkiye

[2] Department of Chemical Engineering, Çankırı Karatekin University, Çankırı 18100, Türkiye

Graphical abstract

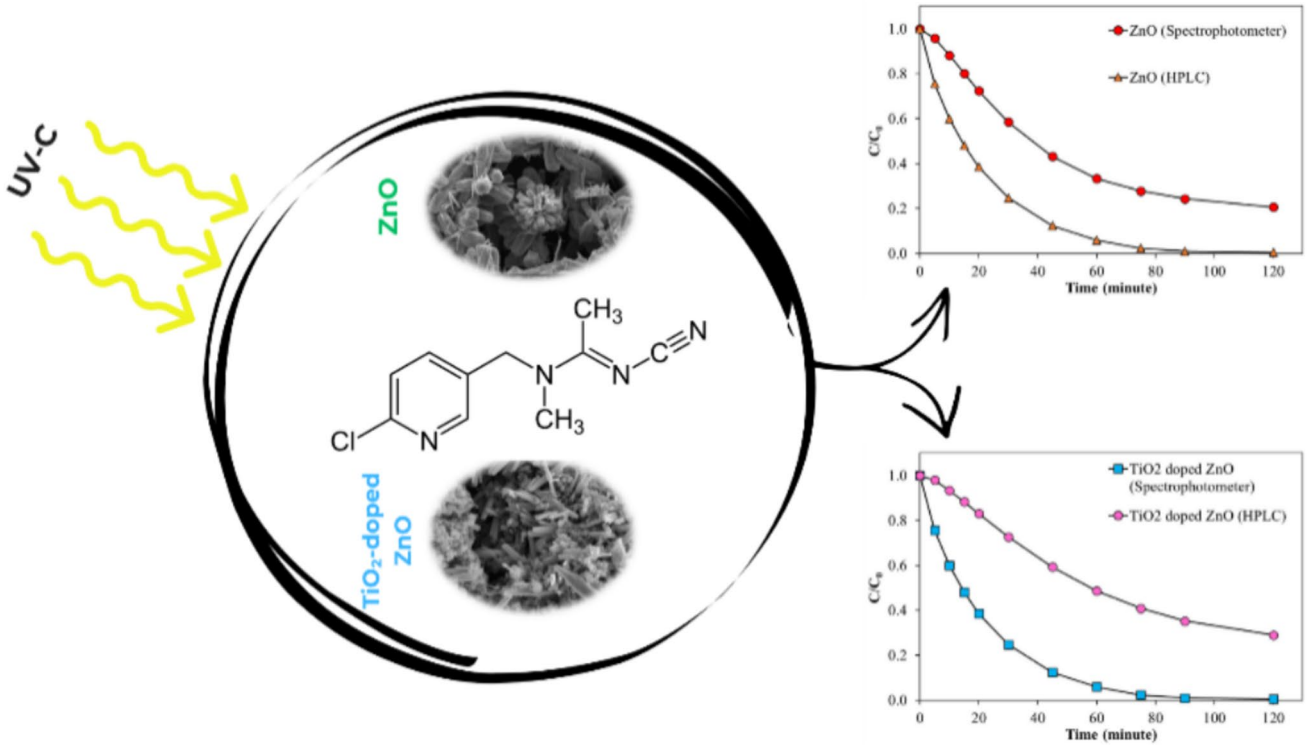

Keywords Crystallization · ZnO · Acetamiprid · Photocatalyst · TiO_2-doped ZnO

Introduction

Pesticides are chemicals used during agricultural production to minimize the damage caused by pests (such as sinsects, viruses, bacteria, rodents, and unwanted plants) (Aslan and İçli 2022). Neonicotinoids are one of the most important classes of insecticides worldwide due to their high efficacy against a wide range of significant insect pests and their diverse applications (Bass et al. 2015). SinceS their introduction in the 1990s, neonicotinoids have been extensively used in agricultural production and for the protection of landscape plants from pests, constituting a significant portion of the global insecticide market (Cui et al. 2024). Currently, neonicotinoids are licensed for use in over 140 types of products across 120 countries. There are seven main types of neonicotinoids, which are effective against many sucking pests, as well as some coleopteran, dipteran, and lepidopteran species, through foliar, soil, and seed applications (Elbert et al. 2008). These include imidacloprid (IMI), thiamethoxam (THM), clothianidin (CLO), dinotefuran (DIN), acetamiprid (ACE), thiacloprid (THI), and nitenpyram (NTP) (Bass et al. 2015). Neonicotinoids have a wide range of applications due to their high toxicity to insects and low toxicity to vertebrates, as well as their high solubility in water (Zhang et al. 2024a). However, they can easily enter aquatic environments through surface runoff or infiltration into groundwater and be absorbed by animals and plants. This is because only 20% of the active chemicals are absorbed by plants, while the remaining 80% is released into the environment (Tsegay et al. 2024). It has been reported that neonicotinoids have toxic effects in aquatic ecosystems, particularly on fish, invertebrates, and other aquatic organisms, leading to adverse outcomes such as behavioral changes, reproductive issues, and death. This situation can also affect the food chain, causing ecosystem imbalances and a decline in biodiversity (James et al. 2016). Global monitoring studies have indicated that neonicotinoid residues exceeded this threshold in 73.6% of surface water samples, with concentrations reaching as high as 100.0–400.0 µg/L in some cases (Cui et al. 2024). Morrissey et al. (2015) reported that neonicotinoid concentrations in water exceeding 0.035 µg/L or

short-term high exposures exceeding 0.2 µg/L could be harmful to sensitive aquatic invertebrates. Additionally, it has been suggested that these chemicals are persistently transported into water bodies from agricultural areas and urban environments, posing serious negative impacts on aquatic ecosystems (Morrissey et al. 2015). The potential effects of neonicotinoids on human health have been linked to neurological disorders and negative impacts on the endocrine system. Moreover, the bioaccumulation of these chemicals carries the risk of entering the food chain through aquatic organisms, ultimately reaching humans (James et al. 2016).

ACE is one of the most effective and widely used neonicotinoid insecticides for controlling various insect pests (Zbiljić et al. 2015). Unlike other neonicotinoids, ACE has a unique mechanism of action that is effective against both Hemiptera and Thysanoptera, as well as Lepidoptera, offering significant potential for managing resistance development and providing environmental safety features, making it an important alternative for agricultural pest control (Yamada et al. 1999). ACE negatively affects the immune system, ion balance, and behavior in mammals, leading to organ system toxicity, oxidative stress, and DNA damage, while also causing cytotoxicity and apoptosis in brain tissue along with various physical symptoms, posing significant risks to human health (Phogat et al. 2022). Due to its high solubility and widespread use, it presents potential risks to human health and aquatic organisms. The European Union has included five neonicotinoid insecticides, including ACE, in the Watch List of potential hazardous pollutants (Serrano et al. 2020). Therefore, developing methods for the effective and environmentally friendly removal of ACE from the environment is of great importance (Benhalima et al. 2024).

Various techniques are available for the removal of ACE pesticide from aqueous solutions. These techniques include photocatalytic degradation (Licht et al. 2023; Benhalima et al. 2024; Liu et al. 2024), fungal bioremediation and ozonation (Beltrán-Flores et al. 2024), thermal degradation (Popadić et al. 2023), adsorption (Sellaoui et al. 2023), photobioreactor (Avila et al. 2022), solar photo-Fenton (Soriano-Molina et al. 2018), UV/hydrogen peroxide (UV/H_2O_2) and UV/potassium persulfate (UV/PS) (Chen et al. 2018). Among these methods, photocatalysis has been recognized in recent years as a method aligned with the zero-waste principle due to its sustainability, eco-friendly characteristics, and high efficiency. This process provides an effective solution in water treatment applications, playing a critical role in the removal of pollutants. Photocatalytic processes stand out as an important strategy for cleaning water resources and reducing environmental pollution (Licht et al. 2023).

While TiO_2 stands out as the most important metal oxide semiconductor due to its unique photocatalytic properties, ZnO nanoparticles also attract attention for their low cost and high photocatalytic efficiency (Liu et al. 2023). However, the low natural light absorption efficiency of TiO_2 limits its practical applications (Hashimoto et al. 2005). To enhance TiO_2's visible light absorption, various modification techniques such as non-metal and metal doping, dye sensitization, and semiconductor combinations are used (Pelaez et al. 2012). Metal ion doping improves TiO_2's photocatalytic activity under visible light by narrowing the energy band gap and preventing charge recombination. In particular, doping with metal ions like Cu^{2+}, Ni^{2+}, Zn^{2+}, and Fe^{3+} significantly improves TiO_2's photocatalytic performance, while doping with non-metals such as nitrogen or carbon can further enhance its visible light absorption (Liu et al. 2024; Yang et al. 2024).

ZnO, another widely studied n-type semiconductor, combines a wide band gap, high electron mobility, and transparency to visible light, making it a strong candidate for photocatalytic applications (Berberidou et al. 2016; Ganie et al. 2021; O'Neill et al. 2023; Wang et al. 2023). In wastewater treatment, ZnO has shown high efficiency in degrading organic pollutants and toxic metal ions, and it has been reported to be more effective and cost-efficient than TiO_2 in water disinfection processes (Ahmed and Haider 2018). Its unique properties-such as direct band gap, strong near-UV emission, transparent conductivity, and piezoelectricity-further enhance its suitability for environmental and energy-related applications (Sathishkumar et al. 2016). With these advantages, ZnO stands out as a promising photocatalyst for sustainable and green treatment technologies (Darvishi Cheshmeh Soltani et al. 2016; Tahoun et al. 2022).

There is limited information in the existing literature regarding the removal of ACE from aqueous solutions. Most reported studies have focused on conventional techniques such as adsorption, ozonation, and biological treatments, which often suffer from low efficiency or secondary pollution issues (Ahmed and Haider 2018; Beltrán-Flores et al. 2024). Although photocatalytic processes have been applied to degrade various pesticides, investigations specifically targeting ACE removal remain scarce (Licht et al. 2023; Liu et al. 2024). In this study, the effects of simulated solar light, UV-A, and UV-C irradiation were examined separately, and the impact of parameters such as photocatalyst amount, initial ACE concentration, and initial pH on removal efficiency was evaluated. The study also investigated the role of ZnO and TiO_2-doped ZnO photocatalysts in the degradation mechanisms of ACE and its environmental implications. By

addressing the current research gap, this work provides new insights into the photocatalytic oxidation of ACE, offering a scientific foundation for environmentally friendly treatment technologies and significantly contributing to the existing literature. Additionally, novel ZnO and TiO_2-doped ZnO photocatalysts were synthesized in this work and comprehensively characterized using FESEM, EDX, XRD, FT-IR, and XPS techniques. The ACE degradation efficiency was monitored using UV–Vis spectrophotometry, while intermediate and final degradation products were identified through LC–MS/MS and HPLC analyses.

Materials and methods

Equipment and chemicals

Zinc Nitrate Hexahydrate ($Zn(NO_3)_2{\cdot}6H_2O$), Titanium Dioxide (TiO_2), and Hexamethylenetetramine ($C_6H_{12}N_4$) were purchased from Sigma. ACE Hekplan 20 SP ($C_{10}H_{11}ClN_4$) was purchased from Hektaş. Sodium Hydroxide (NaOH) and 98% Sulfuric Acid (H_2SO_4) were purchased from Merck. Magnetic stirring processes were carried out using a Heidolph MR Hei-TEC magnetic stirrer with heating plate. The quantities of chemicals were determined using an A&D HR-250 precision balance.

Experimental

In the synthesis of ZnO and TiO_2-doped ZnO photocatalysts and in the experiments for the removal of ACE from aqueous solutions, a circular, high-light-transparency, double-walled glass reactor was used. A refrigerated circulator was employed to control the temperature within the reactor. Stirring was carried out using a magnetic stirrer positioned beneath the reactor. In the photocatalytic ACE removal experiments, the simulated solar light lamp and the UV-A and UV-C lamps were placed inside a quartz tube and positioned within the reactor. To separate the catalyst from the suspensions in the samples, the samples were centrifuged at 14,000 rpm for 15 min at 15 °C. The light source was turned on about 15 min before being placed into the reactor to reach a stable light intensity. Additionally, the outer parts of the reactor were covered with aluminum foil to prevent light loss. In the photocatalytic process for the removal of ACE, laboratory-prepared aqueous solutions of ACE at defined concentrations were used, and the effects of parameters such as initial solution pH (3–11), catalyst amount (0.25–1.5 g), and initial ACE concentration (5–20 mg/L) on pollutant removal were investigated. The reaction time for each experiment was 120 min, and samples were taken and immediately analyzed at specified time intervals. A 0.1 M H_2SO_4 or NaOH solution was used to adjust the initial pH values. The experimental setup for photocatalytic experiments and synthesis is shown in Fig. 1.

During the experiments, ACE concentrations were determined immediately after sampling by measuring absorbance values using a UV–Vis spectrophotometer (Shimadzu, UV-1800) at the maximum wavelength (254 nm) with a calibration curve prepared beforehand. The relative concentration (C/C_0) of ACE was calculated using Eq. 1.

$$\text{Relative concentration of } ACE = C/C_0 = C_t/C_0 \quad (1)$$

Here, C_0 represents the initial concentration of ACE, and C_t represents the ACE concentration at any given time.

In the photocatalytic experiments, each test was repeated three times under identical conditions, and mean values with standard deviations (± SD) are reported in the tables to ensure accuracy and reproducibility of the data.

Synthesis of ZnO and TiO_2-doped ZnO

The synthesis of ZnO and TiO_2-doped ZnO was carried out using homogeneous hydrolysis through low-temperature crystallization. A typical synthesis procedure for ZnO is as follows: Zinc nitrate hexahydrate and hexamethylenetetramine solutions were prepared in equimolar amounts, and the concentration was set to 0.03 M. These solutions were mixed in the reactor, with the reaction time set to 2 h. ZnO was synthesized using the chemicals according to the reaction equations given in Eqs. (2), (3), and (4) (Akin and Oner 2012).

$$(CH_2)_6N_4 + 6H_2O \rightarrow 6HCHO + 4NH_3 \quad (2)$$

$$NH_3 + H_2O \rightarrow NH_4^+ + OH^- \quad (3)$$

$$Zn^{+2} + 2OH^- \rightarrow ZnO + H_2O \quad (4)$$

The overall reaction equation obtained by summing the reactions is presented in Eq. (5).

$$2Zn(NO_3)_2 + C_6H_{12}N_4 + 8H_2O \rightarrow 2ZnO\downarrow + 4NH_4NO_3 + 6HCHO \quad (5)$$

The metal oxide TiO_2, used as a dopant, is added to the environment before the reaction begins, and the resulting ZnO material accumulates on the TiO_2 surface during the reaction. The solution was filtered using filter paper with a pore size of 0.22 µm. The crystals obtained by filtration after the reaction were dried under vacuum at 60 °C for approximately 24 h.

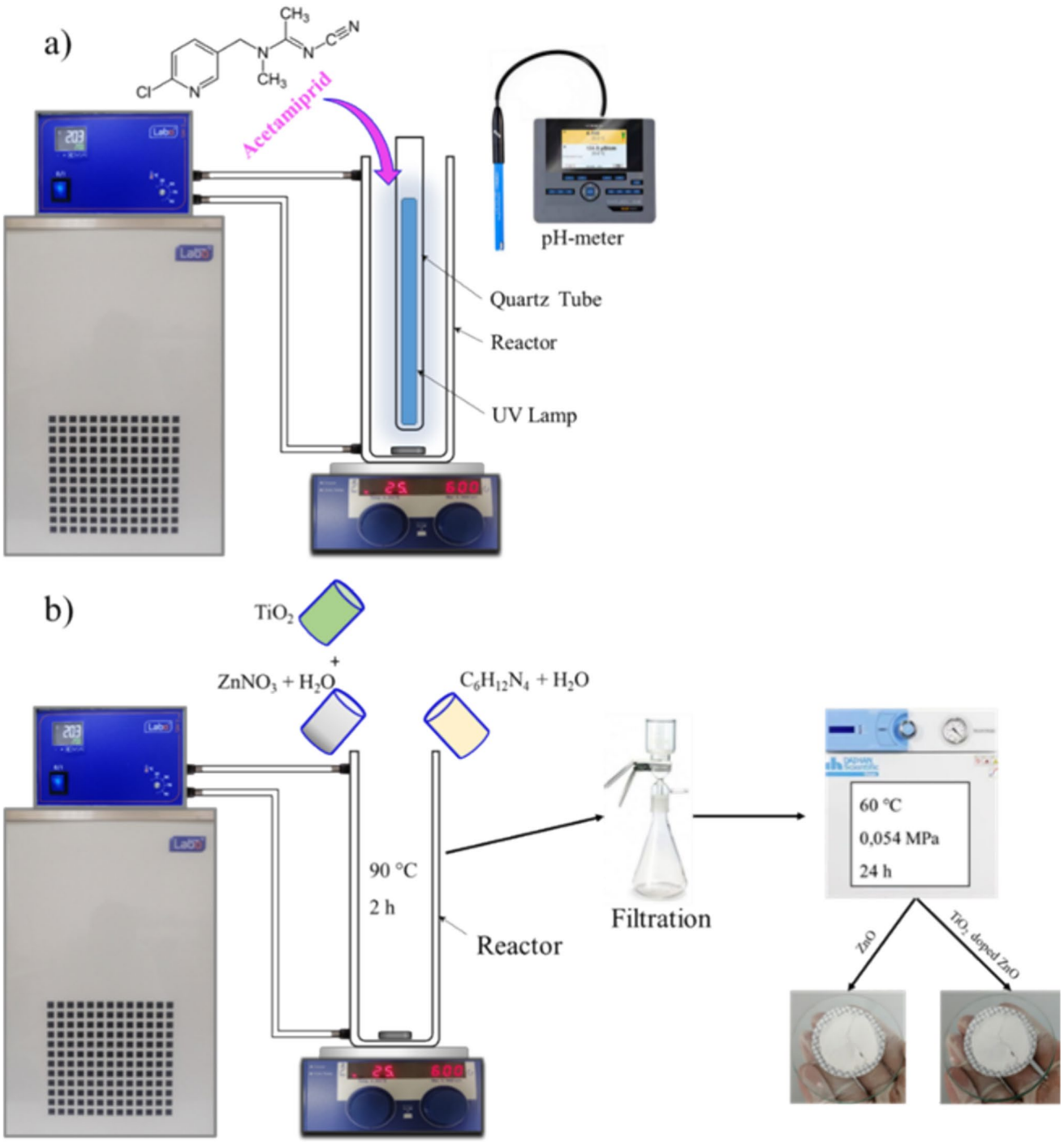

Fig. 1 Photocatalytic experimental setup (**a**) and Experimental setup used for the synthesis of ZnO and TiO_2-doped ZnO (**b**)

Kinetic model

A pseudo-first-order kinetic model of photocatalytic degradation for different concentrations of ACE was used (Vasanth Kumar et al. 2007). In the literature, it has been noted that the linear forms of kinetic models can lead to erroneous results and thus incorrect decisions, depending on the data used. In contrast, non-linear forms are reported to provide a better fit to experimental data (Lin and Wang 2009; Lima et al. 2015; Simonin 2016). Therefore, a non-linear method was used in the solution of the kinetic model (Tran et al. 2017). The coefficients for the models used were calculated using the non-linear method with the help of the Solver plug-in in Microsoft Excel. The kinetic model, R^2, and chi-square (X^2) values were calculated using the Eqs. (6–8) below.

$$\ln\left(\frac{C_{\exp}}{C_0}\right) = -k \times t \tag{6}$$

$$X^2 = \sum \frac{\left(C_{\exp} - C_{est}\right)^2}{C_{est}} \tag{7}$$

$$R^2 = 1 - \frac{\sum \left(C_{\exp} - C_{est}\right)^2}{\sum \left(C_{\exp} - C_{mean}\right)^2} \tag{8}$$

In the equations, C_0 represents the initial concentration of ACE before photocatalytic degradation, C_{exp} represents the concentration of ACE at time t after photocatalytic degradation, C_{est} represents the concentration obtained using the Microsoft Excel Solver plug-in, t is the reaction time, and k is the reaction rate constant.

Characterization

The morphology of ZnO and TiO_2-doped ZnO was analyzed using a scanning electron microscope (FESEM, model Quanta FEG 250) operated at 15 kV. The elemental composition of the photocatalysts was determined by Energy Dispersive X-ray Spectroscopy (EDX) attached to the FESEM, which confirmed the presence and distribution of Zn, Ti, and O elements in the samples. The crystalline structure of ZnO and TiO_2-doped ZnO was analyzed using X-Ray Diffraction (XRD). The measurements were performed using a Bruker D8 Advance X-ray powder diffractometer with a Cu Kα radiation source ($\lambda = 0.154$ nm). The scanning speed was set at 2°/min, and the scan was performed with an increasing 2θ angle between 5° and 90°.

The surface functional groups of ZnO and TiO_2-doped ZnO were analyzed using an ATR-FTIR (Attenuated Total Reflectance Fourier Transform Infrared) spectrometer in the wavelength range of 400–4000 cm^{-1} (resolution 4 cm^{-1}, 24 scans).

Identification of Degradation Products and Quantitative Analysis of ACE Using LC–MS/MS and HPLC

LC–MS/MS 8040 liquid chromatography-mass spectrometry (LC–MS/MS) and HPLC analyses were conducted to identify the products formed as a result of photocatalytic degradation. In the experiments, ACE measurements were performed using an HPLC Shimadzu LC-20A Prominence device with an Agilent Eclipse XDB ODS-3 C18 (5 µm, 4.6 × 250 mm) column. A 9-point standard calibration curve was prepared for the determination of ACE using HPLC. Solutions containing initial concentrations of 0–10 mg/L were used to create the calibration curve. HPLC measurements were conducted at 248 nm. The following calibration curve and equation (Supplementary 1) were used in the measurements (Mobile phase A: ddH_2O, Mobile phase B: ACN, Flow rate: 1 mL/min, Detector: SPD-M20A).

Results and discussion

Characterization

The particle size and morphology of pure ZnO were examined using FESEM imaging. As shown in Fig. 2(a), ZnO crystallizes in two distinct morphological forms: (i) hexagonal rod-like structures and (ii) thinner needle-like structures. Particle dimensions were determined by manually measuring the lengths and widths of crystals directly from the FESEM micrographs using the scale bars provided. For each morphology type, 10 randomly selected particles were measured to obtain representative size distributions. Based on these measurements, the hexagonal rod-shaped ZnO particles exhibited an average length of 3.57 ± 1.21 µm and an average width of 0.72 ± 0.28 µm. The needle-like ZnO structures displayed smaller dimensions, with an average length of 1.12 ± 0.18 µm and a width of 0.16 ± 0.08 µm. These well-defined crystal habits are consistent with the typical morphologies reported for wurtzite-type ZnO (Baruah and Dutta 2009; Ekthammathat et al. 2013). Although such ordered crystal structures reflect well-developed crystallinity, morphology alone cannot be used to infer specific

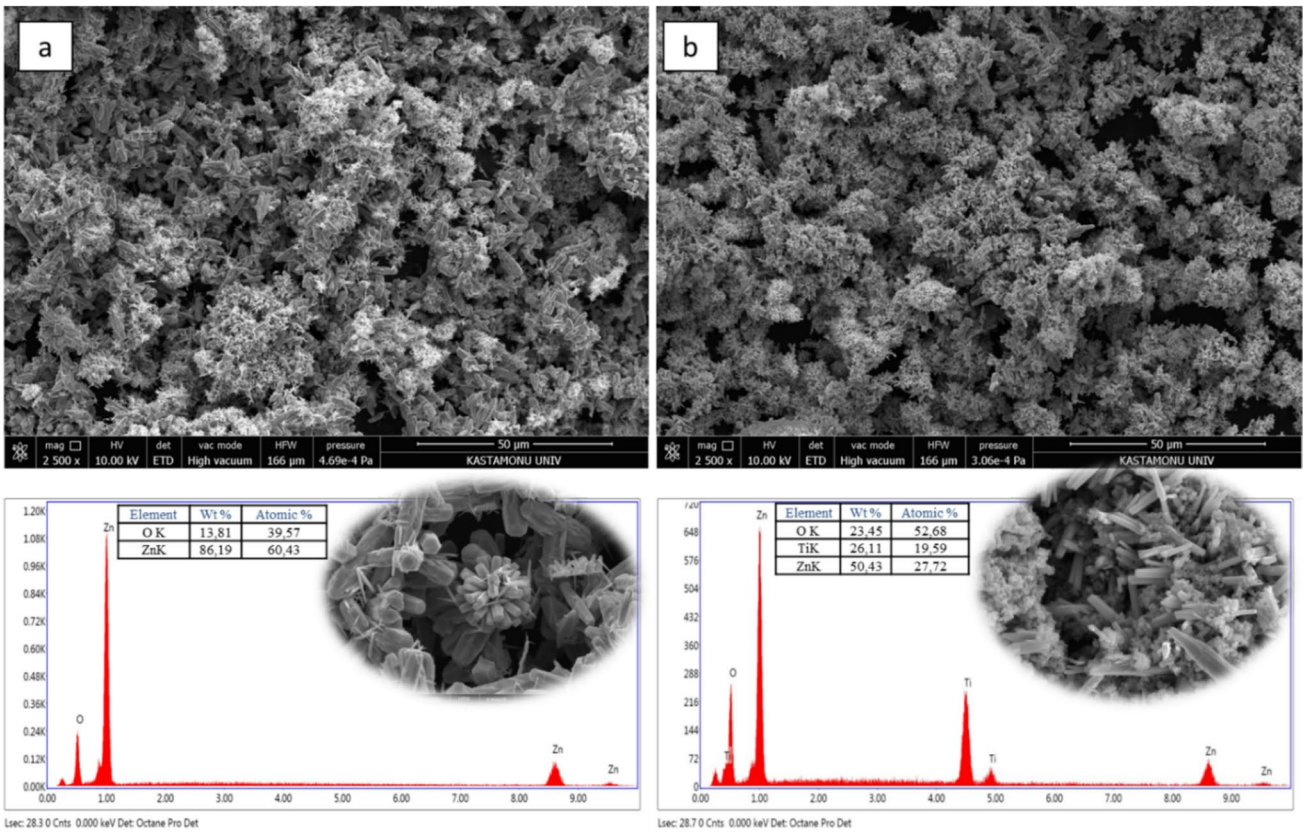

Fig. 2 FESEM images and EDX spectra of ZnO (**a**) and TiO_2-doped ZnO (**b**). Insets show the magnified FESEM images highlighting the particle morphology

surface area; therefore, no surface-area-related interpretation is made here. Higher-magnification FESEM images further revealed the characteristic flower-like assembly of ZnO rods, consistent with previous literature.

In Fig. 2(b), the surface morphology of the TiO_2-doped ZnO sample was examined. The SEM images show that the TiO_2-doped ZnO crystals maintain a hexagonal rod-like structure with a relatively uniform size distribution. In addition, the smaller TiO_2 particles deposited on the ZnO rods can be clearly distinguished due to their spherical appearance (Esfandian et al. 2024). Particle dimensions were determined by manually measuring 10 randomly selected crystals directly from the FESEM micrographs using the scale bars provided. Based on these measurements, the TiO_2-doped ZnO crystals exhibited an average particle length of 1.76 ± 0.44 µm and an average width of 0.30 ± 0.11 µm. The EDX spectra presented in Fig. 2(a–b) confirm the elemental composition of the samples, showing clear signals corresponding to Zn, Ti, and O.

XRD patterns were used to examine the crystal phases, verify the structure, and determine the composition and purity of the synthesized samples. The XRD analyses shown in Fig. 3 reveal the characteristic 2Theta (2θ) peaks of the crystal structure of ZnO in the Zincite phase, as listed in JCPDS card 00–036-1451, at approximately 31.8° (100), 34.4° (002), 36.2° (101), 47.5° (102), 56.6° (110), 62.8° (103), 66.4° (200), 67.9° (112), and 69.2° (201) (Scarano et al. 2006; Asikuzun and Ozturk 2018). These diffraction peaks and the corresponding crystal planes confirm the typical hexagonal wurtzite structure of ZnO (Akin and Oner 2012; Asikuzun and Ozturk 2019) and verify that the crystal phase has been successfully formed (Ahmad et al. 2022).

The XRD analysis of TiO_2 was conducted to examine the crystal phases and verify the structure, and the diffraction pattern obtained revealed that all the peaks correspond to the characteristic peaks of TiO_2 in the Anatase phase, as listed in JCPDS card 01–086-1157. The diffraction peaks observed in this analysis were identified at approximately $2\theta = 25.3°$ (101), 37.8° (004), 48.1° (200), 53.9° (105), 55.1° (211), and 62.8° (204) (Hamdani et al. 2022). The successful matching of these peaks with the corresponding tetragonal crystal planes confirms the presence of the anatase phase of TiO_2 and indicates that the crystal structure has been successfully formed (Esfandian et al. 2024).

When examining the XRD patterns of TiO_2-doped ZnO photocatalysts, it was found that the ZnO phase aligns with

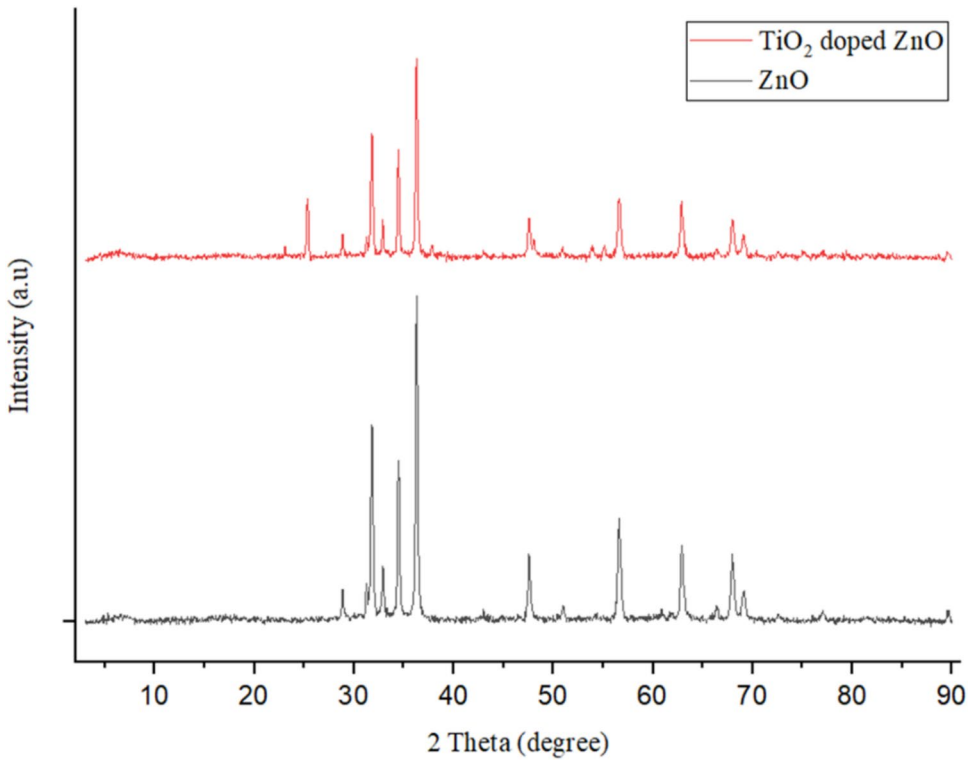

Fig. 3 XRD diffraction pattern of ZnO and TiO_2-Doped ZnO

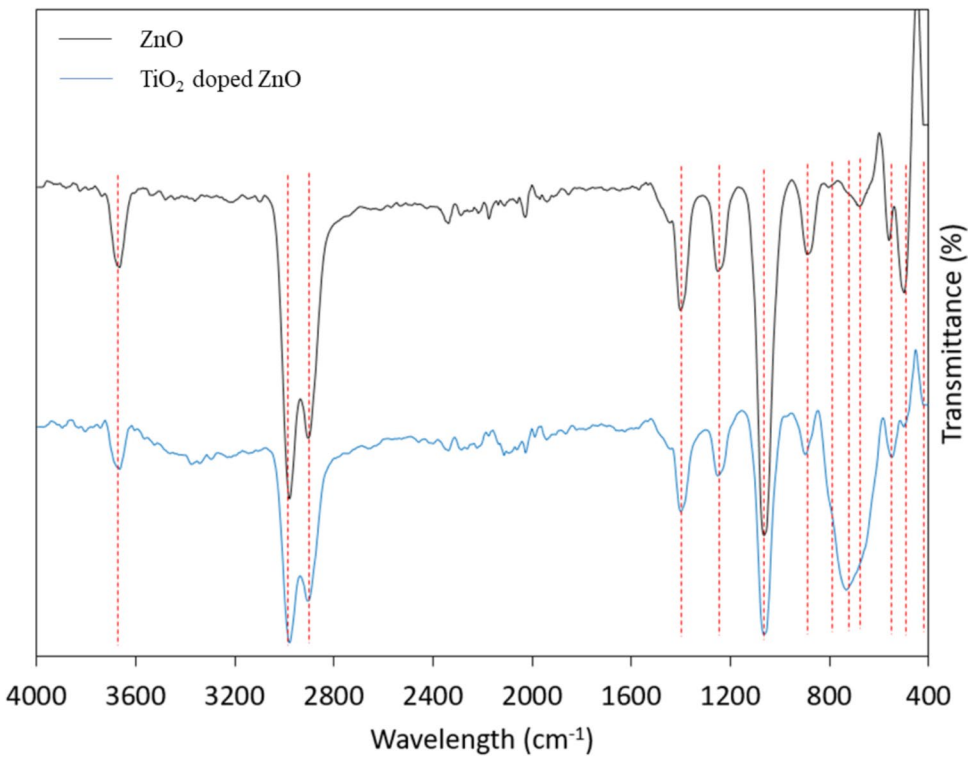

Fig. 4 ATR-FTIR spectra of ZnO and TiO_2-doped ZnO

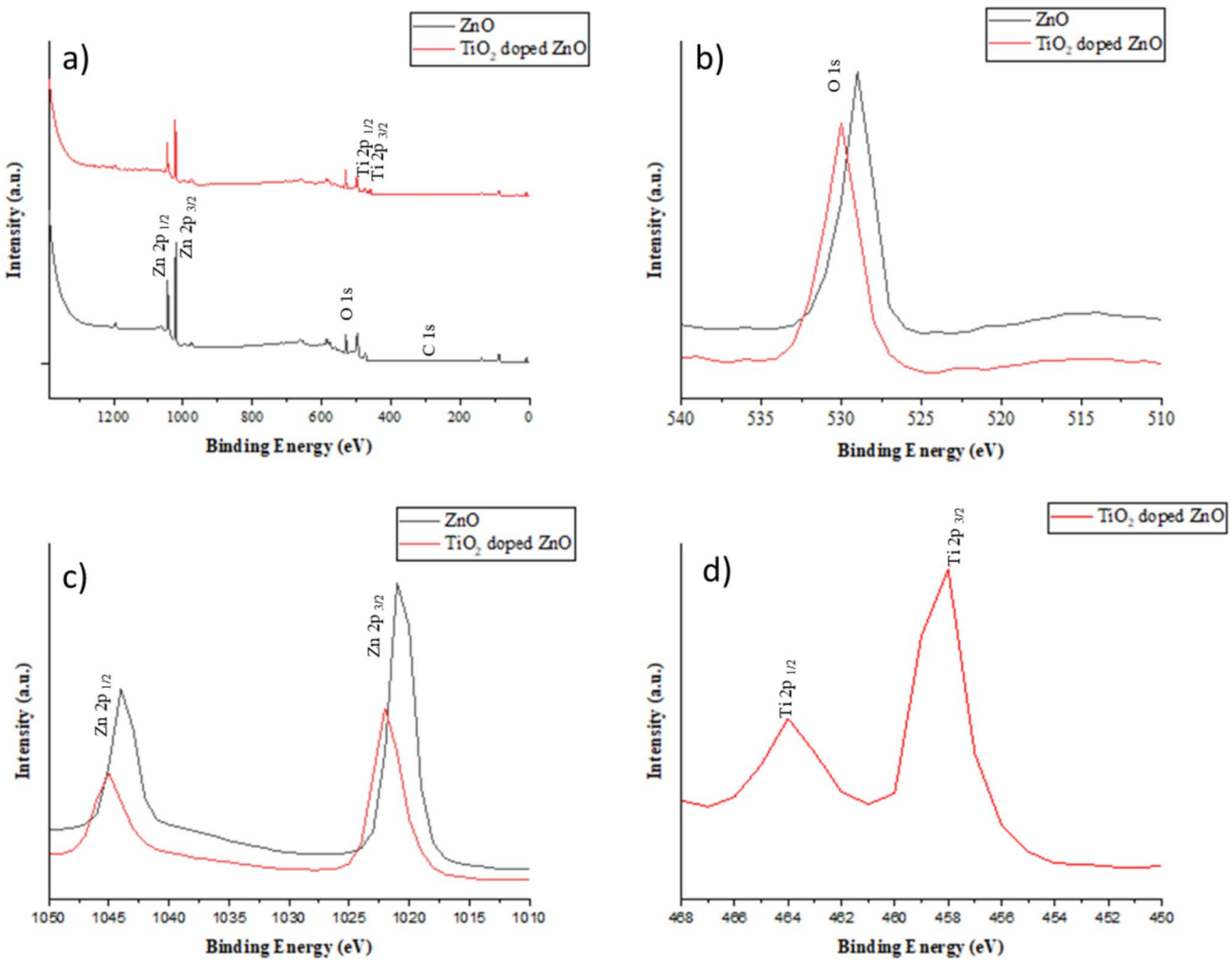

Fig. 5 High-resolution XPS spectra of **a** Survey spectra, **b** O 1 s, **c** Zn 2p, and **d** Ti 2p for the ZnO and TiO_2-doped ZnO

the Zincite pattern, while the TiO_2 phase aligns with the Anatase pattern. This indicates that the TiO_2 doping maintains the crystal structure of ZnO while also contributing with the presence of the anatase phase of TiO_2. This structural alignment shows a reduction in peak intensities when comparing TiO_2-doped ZnO with pure ZnO, suggesting the formation of smaller crystallite sizes. This structure points to improved photodegradation efficiency (Shathy et al. 2022).

Figure 4 shows the ATR-FTIR spectra of pure ZnO and TiO_2-doped ZnO photocatalysts. In the spectrum of pure ZnO, characteristic bands at 542 cm^{-1} and 420 cm^{-1} correspond to Zn–O stretching vibrations, consistent with the wurtzite ZnO structure (Al-Gaashani et al. 2013). In TiO_2-doped ZnO, additional features in the 500–700 cm^{-1} region were observed, which can be assigned to Ti–O-Ti and Zn–O-Ti linkages (Mazabuel-Collazos and Rodríguez-Páez 2018). A broad absorption between 3200–3500 cm^{-1} was attributed to hydrogen-bonded hydroxyl groups or adsorbed water molecules on the surface. In addition, a sharp band at ~ 3700 cm^{-1} was observed, which is characteristic of isolated, non-hydrogen-bonded hydroxyl groups on the ZnO surface. This assignment is in agreement with (Viñes et al. 2014), who demonstrated that such free OH species on ZnO surfaces give rise to distinct sharp absorptions in the 3600–3700 cm^{-1} region. These results indicate that both ZnO and TiO_2-doped ZnO retain surface hydroxyl functionalities, which serve as crucial active sites for the generation of reactive oxygen species (ROS), such as ·OH, $\cdot O_2^-$ and H_2O_2, during photocatalysis. These ROS play a central role

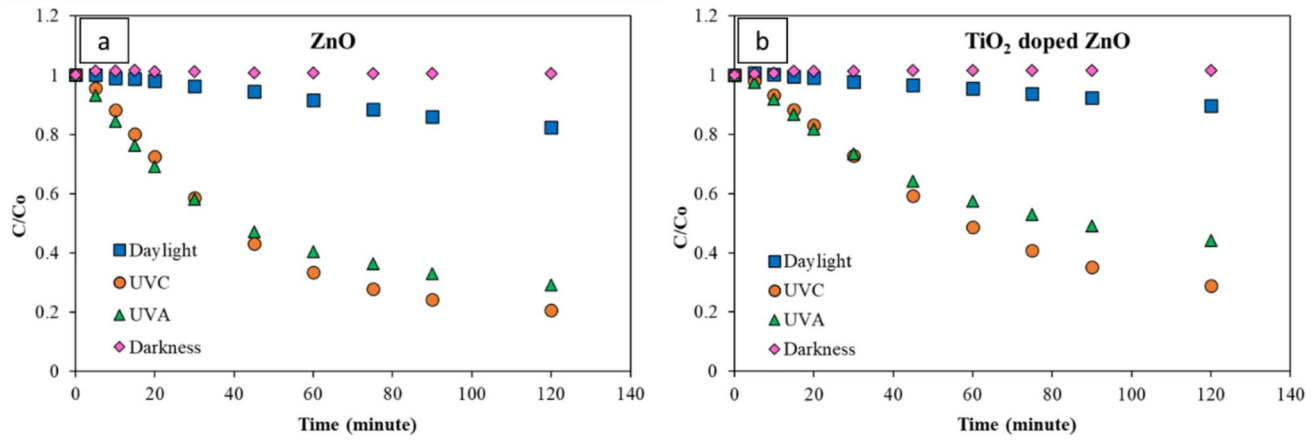

Fig. 6 Effect of different light sources on the removal of ACE by ZnO and TiO_2-doped ZnO photocatalysts (C_0: 5 mg/L, catalyst amount: 1 g/L, T: 20 °C, pH: 6.2, and stirring speed: 650 rpm)

in pollutant degradation by attacking and oxidizing organic molecules.

The elemental composition and valence states of ZnO and TiO_2-doped ZnO photocatalysts were investigated using X-ray photoelectron spectroscopy (XPS). The survey spectrum showed characteristic peaks of O 1 s, C 1 s, Zn 2p, and Ti 2p (Fig. 5), confirming the presence of these elements. Zn 2p core levels displayed two peaks at ~ 1021 eV and ~ 1044 eV corresponding to Zn $2p_{3/2}$ and Zn $2p_{1/2}$ (Al-Gaashani et al. 2013). Ti 2p peaks were observed at 458 eV and 464 eV, confirming Ti^{4+} oxidation state (Papitha et al. 2024). O 1 s peaks at 529 and 530 eV indicated oxygen in metal oxides (Wu et al. 2018). The C 1 s peak at 284 eV was attributed to surface carbon contamination (Ibrahim et al. 2020).

Photocatalytic degradation of ACE

Effect of light source on photocatalytic performance

In this study, the removal of the ACE pollutant using the produced catalysts was investigated, focusing on the parameters affecting oxidation performance. Initially, the catalyst efficiency was examined in a dark environment, followed by investigating the effects of simulated solar light, UV-A, and UV-C on oxidation performance. The impact of the light source over time was studied in solutions with a pollutant concentration of 5 mg/L, a catalyst amount of 1 g/L, a temperature of 20 °C, a stirring speed of 650 rpm, and at their natural pH. The photocatalytic oxidation performance of ACE under dark conditions and different light sources using various photocatalysts is shown in Fig. 6. When evaluating oxidation performance, UV-C light was preferred for both catalysts.

When the adsorption effect of both photocatalysts was examined in a dark environment, no change was observed over 120 min. For the degradation of ACE using ZnO, a removal efficiency of 18% was achieved after 120 min under simulated solar light, 71% under UV-A, and 79% under UV-C. For the degradation of ACE using TiO_2-doped ZnO photocatalyst, the removal efficiency was 10% under simulated solar light, 55% under UV-A, and 71% under UV-C after 120 min. Upon reviewing the results, the photocatalytic degradation performance of ACE with different catalysts under various light sources was found to be UV-C > UV-A > simulated solar light. The obtained performance order is attributed to the wide band gap and high electron mobility of ZnO, together with the UV absorption properties of TiO_2; in this context, the higher photon energy of UV-C leads to more effective e^-/h^+ excitation and ROS generation compared to UV-A and simulated solar light (Gonçalves et al. 2021).

In a study from the literature, it was reported that the photocatalytic reaction mechanisms and charge transfer of TiO_2-ZnO photocatalysts begin during the irradiation of the target compound with visible light. In this process, electrons in the valence band (VB) are excited to the conduction band (CB), and an equal number of holes (h^+) are created. Electrons transfer from ZnO to TiO_2, while holes transfer from TiO_2 to ZnO. These electrons and holes participate in chemical reactions, facilitating the separation of photo-induced electron–hole pairs and reducing the recombination rate. As a result, it has been noted that the photocatalytic properties of TiO_2-ZnO composite photocatalysts are enhanced (Qin et al. 2019). TiO_2-ZnO

heterojunctions significantly enhance photocatalytic activity due to extended visible light absorption and efficient charge separation, thereby enabling high efficiency in the degradation of various pollutants under visible light (Zhang et al. 2024b). However, our findings indicate that under high-energy UV irradiation, TiO_2 doping in the produced photocatalysts has only a limited effect on improving performance, and pure ZnO performs equally well or even better. This result shows that TiO_2 doping does not always guarantee higher photocatalytic efficiency, which is in line with the findings of (Nawaz et al. 2023), who also reported that doping ZnO or TiO_2 with metals or nonmetals is not necessarily favorable for tuning their optical characteristics (such as band gap and light absorption behavior).

The efficiency of TiO_2-doped ZnO under low-energy light conditions is quite limited; only 10% efficiency was achieved under simulated solar light. In a dark environment, neither catalyst showed almost any activity, clearly demonstrating that sufficient light energy is necessary for effective photocatalytic reactions. Under UV-A light, TiO_2-doped ZnO achieved 55% efficiency, while pure ZnO showed 71% efficiency, indicating that TiO_2-doped ZnO is effective only under certain light conditions. In a study investigating the photocatalytic performance of the TiO_2 and ZnO dual system in the degradation of humic substances, it was observed that TiO_2 did not provide the expected level of efficiency increase in the photocatalytic removal of environmental pollutants and, in some cases, fell below the natural efficiency of ZnO. It has been noted that the electron mobility of ZnO ($200-300\ cm^2/Vs$) is significantly higher than that of TiO_2 ($0.1–4.0\ cm^2/Vs$), which allows ZnO to have higher quantum efficiency and better photocatalytic performance. Furthermore, since the valence band of ZnO (VB-ZnO) is located lower than that of TiO_2 (VB-TiO_2), the oxidation potential of the hydroxyl radical produced by ZnO is higher compared to that produced by TiO_2, which enhances ZnO's photocatalytic efficiency (Turkten and Bekbolet 2020). Discrepancies between our results and previously published studies can be attributed to differences in synthesis procedures (e.g., sol–gel vs. hydrothermal), TiO_2 loading ratios, crystallinity, and surface morphology, all of which critically govern interfacial charge-transfer processes and ROS-generation pathways and, in turn, determine the overall photocatalytic efficiency (Akhter et al. 2023). Consistent with previous studies, ZnO frequently demonstrates superior photocatalytic performance compared to TiO_2, attributable to physicochemical factors including crystallinity, particle size, specific surface area, impurity concentration, and optical characteristics (Fenoll et al. 2015).

To further clarify the photocatalytic behavior, the degradation mechanism of ACE in the presence of ZnO and TiO_2-doped ZnO was also considered (Guzsvány et al. 2009, 2012). Based on LC–MS/MS analysis and supporting literature, it is proposed that ACE degradation proceeds through the generation of reactive oxygen species (ROS), including hydroxyl radicals ($OH^•$), superoxide radicals ($O_2^{•-}$), and photogenerated holes (h^+). For pure ZnO, hydroxyl radicals are important species that promote hydroxylation of the aromatic ring and dealkylation of side chains (Saury Miyashiro and Hamoudi 2021; Zelić et al. 2022). In the case of TiO_2-doped ZnO, TiO_2 improves charge separation and reduces electron–hole recombination, increasing ROS production (Prabhu et al. 2024; Zhang et al. 2024b). As a result, additional degradation pathways-such as cyano-group cleavage and (more tentatively) N-oxidation are observed (Guzsvány et al. 2009, 2012). These results suggest that TiO_2 doping modifies ZnO's surface/electronic properties, leading to a slightly altered route compared to pure ZnO (Zhang et al. 2024b).

Effect of pH on photocatalytic performance

pH plays a critical role in photocatalytic reactions in water treatment. The surface charge of the photocatalyst changes depending on the pH level. The optimal pH for the photodegradation process is related to the point of zero charge (pHpzc) of the photocatalyst. In this context, the effects of pH on photocatalytic efficiency vary depending on the type of photocatalyst used and the target pollutant (AlMohamadi et al. 2024).

In this study, the effect of pH on the photocatalytic degradation of ACE was investigated at pH levels of 3, 7, 9, 11, and 6.2 (solution pH). As seen in Fig. 7, pH had a significant impact on the photocatalytic degradation of ACE when different catalysts were used. For each catalyst used in the experiments, the most effective pH was found to be the natural pH of the pollutant's water solution, which is 6.2. In photocatalytic degradation experiments conducted at this natural pH of 6.2 over 120 min, a removal efficiency of 79% was achieved with the ZnO catalyst, and 71% with the ZnO-TiO_2 catalyst.

Due to the nonionic structure of ACE, it cannot bind to the photocatalyst through protonation or deprotonation processes (Wang et al. 2016). The point of zero charge (PZC) of ZnO is around pH 9; below pH 9, the ZnO surface is positively charged, and above pH 9, it is negatively charged (Vidya et al. 2020). The PZC range of TiO_2 typically varies between 4.5 and 7. The surface charge of TiO_2 also changes depending on the pH: when the pH is above the PZC, the surface is negatively charged, and when it is below, it is positively charged (AlMohamadi et al. 2024). Considering the surface properties of ZnO and TiO_2, it is understood that at pH 6.2, nonionic ACE reacts effectively with reactive oxygen species, independently of electrostatic interactions with the photocatalyst surface (Kosmulski 2002, 2020; Garber and Steeger 2008; Nosaka and Nosaka 2017). In particular, hydroxyl radicals formed at

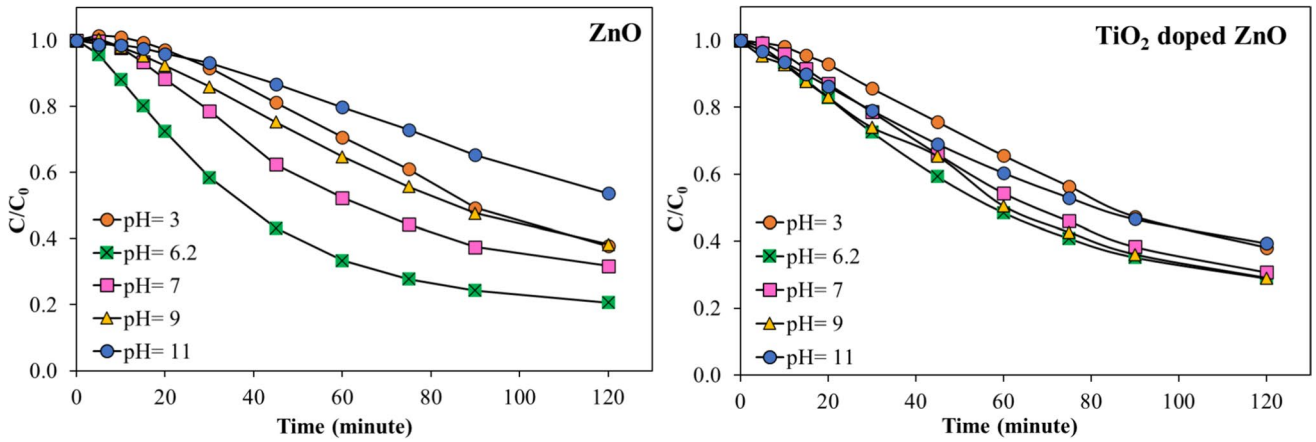

Fig. 7 Photocatalytic degradation of ACE by ZnO and TiO_2-doped ZnO at different pH levels (C_0: 5 mg/L, catalyst amount: 1 g/L, T: 20 °C, UV-C, and stirring speed: 650 rpm)

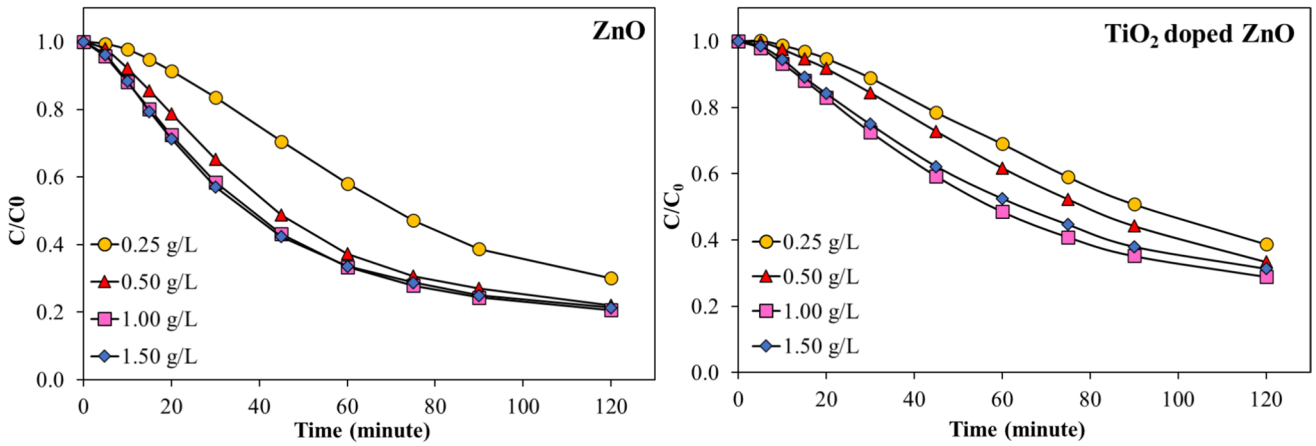

Fig. 8 Photocatalytic degradation of ACE by ZnO and TiO_2-doped ZnO at different catalyst dosages (C_0: 5 mg/L, pH: 6.2, T: 20 °C, UV-C, and stirring speed: 650 rpm)

pH 6.2 are thought to play a key role in this high degradation efficiency. The photocatalytic reactions of the ZnO/TiO_2 suspension system in an aqueous medium can be described as follows (Anil and Surenjan 2024).

$$ZnO + h\nu(< 380nm) \rightarrow h^+ + e^- \quad (9)$$

$$TiO_2 + h\nu(< 380nm) \rightarrow h^+ + e^- \quad (10)$$

$$h^+ + OH^-_{(surface)} \rightarrow OH^\bullet \quad (11)$$

$$h^+ + H_2O \rightarrow OH^\bullet + H^+ \quad (12)$$

$$OH^\bullet + ACE \rightarrow \text{degradation products} \quad (13)$$

Effect of ZnO and TiO_2-doped ZnO catalyst amount on photocatalytic performance

In photocatalytic processes, catalyst dosage is a critical parameter that determines the degradation efficiency of organic pollutants. An increase in catalyst dosage enhances the production of reactive radicals by creating more active surface area, thereby accelerating photodegradation. However, when a certain optimal dosage is exceeded, light scattering and agglomeration of catalyst particles occur, which reduces photocatalytic efficiency. Therefore, determining the optimal catalyst concentration is important to maximize photocatalytic efficiency (AlMohamadi et al. 2024).

In our study, UV-C light was used as the ultraviolet light source for the removal of ACE, and experiments were carried out under fixed conditions with an initial concentration of 5 mg/L, temperature of 20 °C, stirring speed of 650 rpm,

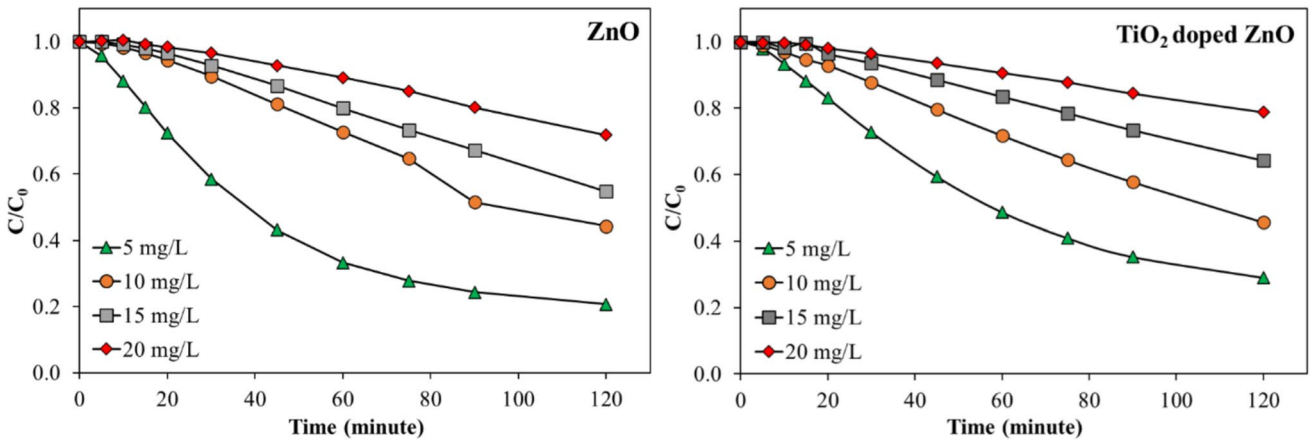

Fig. 9 Photocatalytic degradation of ACE by ZnO and TiO_2-doped ZnO at different catalyst dosages (catalyst dosage: 1 g/L, pH: 6.2, T: 20 °C, UV-C, and stirring speed: 650 rpm)

and natural pH conditions (pH = 6.2). The effects of photocatalytic degradation were examined by adding different amounts of catalyst (0.25, 0.5, 1, and 1.5 g/L). As seen in Fig. 8, the photocatalytic degradation of ACE increased with the addition of ZnO and TiO_2-doped ZnO catalysts, but this increase remained constant after 1 g/L. Therefore, the optimal catalyst amount for both photocatalysts was determined to be 1 g/L. Increasing the catalyst loading causes an increase in solution turbidity, leading to light scattering and reducing the photoactivated volume. Additionally, high catalyst concentrations lead to particle agglomeration, disrupting the homogeneity of the solution and reducing the number of active sites. This results in decreased photocatalytic efficiency and a reduction in process performance (Taie et al. 2021). Other studies in the literature support these findings. Sawunyama et al. (2023) reported that using a catalyst dosage of 0.1 and 0.125 g/L, the UV/B TiO_2-ZnO process removed 63% to 74% of tetracycline (TC) in 120 min (Sawunyama et al. 2023). Habib et al. (2013) also reported that they achieved approximately 98% removal of the azo dye brilliant golden yellow at around pH 7 using 6 g/L of ZnO-TiO_2 nanocomposite in 120 min (Habib et al. 2013). In another study, a maximum efficiency of 92.3% was obtained for chlorpyrifos removal within 140 min using a nanocomposite dosage of 4 g/L (Esfandian et al. 2024). In a different study, a maximum efficiency of 98.7% was achieved for acid blue 25 removal in 150 min with a catalyst dosage of 2 g/L (Yusuff et al. 2024).

Effect of initial ACE concentration on photocatalytic performance

The effect of ACE concentration on removal efficiency was studied by adding 1 g/L of ZnO and TiO_2-doped ZnO to ACE solutions of 5, 10, 15, and 20 mg/L, using UV-C light as the light source at a constant pH of 7 for 120 min. As seen in Fig. 9, the removal efficiency decreased as the ACE concentration increased. Therefore, an initial concentration of 5 mg/L was selected as optimal. Photocatalytic removal efficiency increases with the pollutant's initial concentration up to a certain level, after which the efficiency decreases with further concentration increases. For instance, as seen in the graph in Fig. 9, the degradation efficiency of ACE at a concentration of 5 mg/L approaches 80% in 120 min, while at 20 mg/L, the efficiency falls below 50%. This observation indicates that photocatalytic efficiency significantly decreases at higher concentrations. This decline can be explained by several factors: (1) At higher concentrations, pollutant molecules saturate the active sites of the photocatalyst, keeping the production of reactive species ($OH^{\bullet}$ and $O_2^{\bullet-}$) constant, thereby slowing the degradation rate. (2) The formation of intermediate products, which adsorb onto the active sites, competes with pollutant molecules and reduces the effectiveness of the photocatalyst. (3) A high concentration of pollutants reduces the number of photons absorbed by the photocatalyst surface, leading to a decrease in reactive species production (Mohsenzadeh et al. 2019). Similarly, Mohsenzadeh et al. (2019) reported that high pollutant concentrations reduce the efficiency of the photocatalyst as pollutants occupy the active sites. Another study reported that the occupation of active sites by tetracycline ions reduces the number of hydroxyl radicals formed on the catalyst surface, thus decreasing photocatalytic activity (Sawunyama et al. 2023). As a result, 5 mg/L was chosen as the optimal initial concentration because it offers higher photocatalytic degradation efficiency. At higher initial concentrations, the efficiency decreases due to limitations in photocatalytic reaction mechanisms.

Table 1 Kinetic constants (k) and correlation coefficients (R^2) for the photocatalytic degradation of ACE using synthesized ZnO and TiO_2-doped ZnO catalysts, calculated according to the pseudo-first-order kinetic model ($\ln(C_0/C)$ vs. t)

Concentration (mg/L)	Synthesized ZnO		TiO_2-doped ZnO	
	k (min^{-1})	R^2	k (min^{-1})	R^2
5	0.0171	0.988	0.0118	0.994
10	0.0068	0.972	0.0063	0.990
15	0.0048	0.976	0.0037	0.983
20	0.0027	0.970	0.0020	0.988

Kinetic calculations

Kinetic models are commonly applied to describe the photocatalytic degradation process, relating the degradation rate of the pollutant to the presence and activity of the catalyst (Murugesan et al. 2021). In this study, the photocatalytic degradation of ACE under UV-C light using ZnO and TiO_2-doped ZnO catalysts, synthesized at different initial concentrations (catalyst amount: 1 g/L, stirring speed: 650 rpm, pH 6.2, temperature: 20 °C), was found to follow a pseudo-first-order kinetic model due to the high R^2 values ($R^2 \geq 0.97$). This model is used to explain reactions that occur at a constant rate, independent of the reactant concentration. The experimental results fit this model, allowing for the calculation of kinetic constants.

As the initial pollutant concentration increased, the k values were observed to decrease from 0.0171 to 0.0027 for ZnO and from 0.0118 to 0.0020 for TiO_2-doped ZnO. This decrease is attributed to the saturation of active sites on the catalyst surface as the initial pollutant concentration increases in experiments conducted with a constant catalyst amount. Similarly, the literature indicates that increasing pollutant concentration reduces the reaction rate (Hashemi Monfared and Jamshidi 2019). In the study by Murugesan et al. (2021), a similar decrease in k values was observed with an increase in initial pollutant concentration, and this decrease was explained by the need for more catalytic surface in the solution.

Additives can affect the reaction rate by altering the surface area, active sites, and electronic properties of ZnO. A higher kinetic constant indicates a faster reaction and thus a more efficient catalyst (Premalatha and Rex 2024). Table 1 shows the kinetic constants and R^2 values for the photocatalytic degradation of ACE at different initial concentrations. In both ZnO and TiO_2-doped ZnO catalysts, a decrease in k values and a reduction in photocatalytic degradation rate were observed as the initial concentration increased. This result can be explained by the decrease in light penetration at higher concentrations and the limited availability of active sites on the catalyst surface. The fact that TiO_2-doped ZnO has lower k values compared to pure ZnO demonstrates the effect of TiO_2 on ZnO's photocatalytic efficiency. However, this does not always translate to an increase in reaction rate. This situation may be due to excessive amounts of dopant ions triggering intrinsic point defects that can act as recombination centers, thereby reducing photocatalytic activity (Pan et al. 2020).

Photocatalytic oxidation of ACE with ZnO and TiO_2-doped ZnO photocatalysts: investigation of degradation mechanisms over time using HPLC and LC–MS/MS

In this study, the photocatalytic oxidation process of ACE with ZnO and TiO_2-doped ZnO photocatalysts was investigated. HPLC analyses were conducted to determine the rate

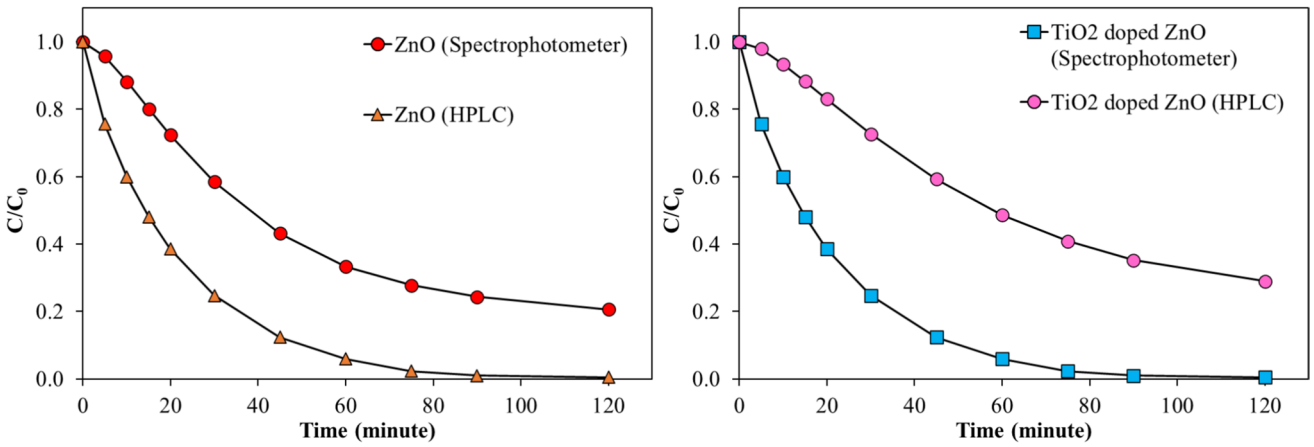

Fig. 10 Comparison of ACE removal with ZnO and TiO_2-doped ZnO catalysts under optimal conditions using HPLC and spectrophotometric analysis (C_0: 5 mg/L, catalyst dosage: 1 g/L, pH: 6.2, T: 20 °C, UV-C, and stirring speed: 650 rpm)

and efficiency of ACE's photocatalytic degradation. In the HPLC analyses performed under optimal experimental conditions, the theoretical retention time of ACE was found to be between 2.773 and 2.778 min. Observations over a period of 120 min revealed that ACE was completely degraded, and the photocatalysts exhibited high efficiency.

As shown in Fig. 10, when comparing the HPLC results with UV spectrophotometer results, it was found that HPLC showed 100% removal, while the UV spectrophotometer results indicated a removal efficiency of 79% for ZnO and 71% for TiO_2-doped ZnO. This difference is thought to be due to the UV spectrophotometer detecting intermediate products formed during the photocatalytic process. The fact that HPLC detects only the main compound may explain the higher efficiency. When comparing the removal rates of ACE, TiO_2-doped ZnO exhibited a slower removal rate compared to pure ZnO.

LC–MS/MS analyses were conducted to identify the intermediate products formed as a result of the photocatalytic oxidation of ACE with ZnO and TiO_2-doped ZnO photocatalysts. In this study, which comparatively examined ZnO and TiO_2-doped ZnO photocatalysts, various by-products emerged over time during the photocatalytic oxidation process of ACE.

The photocatalytic oxidation of ACE under the ZnO catalyst was monitored in detail using mass spectrometry (LC–MS/MS), and intermediate products and final mineralization products formed during the process were identified. Initially, the m/z = 223 peak, corresponding to the main molecule of ACE (Cruz-Alcalde et al. 2017), was observed at the highest intensity, indicating that the photocatalytic reaction had not yet started at this stage. At 15 min, while the peak of the main compound was still present, the appearance of the m/z = 173 peak showed that intermediate products had started to form and the photocatalytic oxidation process had begun. The m/z = 173 peak is likely associated with N-(6-chloropyridin-3-yl) formamide. At 30 min, as the degradation progressed, the formation of larger intermediate products, such as m/z = 164.90 and m/z = 205.05 (ACE-N-desmethyl) (Cruz-Alcalde et al. 2017) was observed, indicating the presence of more complex oxidation intermediates. By 60 min, the main peak of ACE had almost completely disappeared, leaving only the peaks of degradation products. The intensities of peaks like m/z 173, 205, and 248 showed that the reaction had progressed significantly and that ACE had largely degraded. This indicates that the structure of ACE had broken down into smaller fragments and the mineralization process had accelerated. At 120 min, as the photocatalytic reaction progressed, smaller final products with lower toxicity potential were detected. The m/z = 102.90 peak was associated with the presence of TP158, corresponding to 6-chloronicotinic acid. This compound has previously been reported in the literature as a typical intermediate product in the oxidation processes of neonicotinoid insecticides (Carra et al. 2015). These findings demonstrate that ACE was effectively degraded during the photocatalytic oxidation process, and the organic pollutant was transformed into environmentally benign products.

The photocatalytic oxidation of ACE under the TiO_2-doped ZnO photocatalyst was monitored using mass spectrometry (LC–MS/MS), and the formation of intermediate products was observed throughout the process. At 0 min, the m/z = 223 and m/z = 244 peaks corresponding to the main molecule of ACE were detected at high intensity, indicating that the photocatalytic reaction had not yet begun. At 15 min, as the degradation process of ACE started, a decrease in the m/z = 223 and m/z = 244 peaks was observed, and peaks corresponding to intermediate products, such as m/z = 205, m/z = 245, and m/z = 248.90, began to appear. These peaks indicate that the photocatalytic degradation of ACE was progressing.

At 30 min, the main peaks of ACE, m/z = 223 and m/z = 244, had further weakened, while more complex intermediate products, such as m/z = 230, m/z = 246, and m/z = 249, had formed. Among these intermediate products, the m/z = 205 peak can be associated with ACE-N-desmethyl (Cruz-Alcalde et al. 2017). This product is a typical intermediate formed during the photocatalytic oxidation of ACE. By 60 min, the m/z = 223 and m/z = 244 peaks had almost completely disappeared, replaced by larger degradation products such as m/z = 230.85, m/z = 248.85, and m/z = 266.80. At 120 min, the characteristic peaks of ACE had completely vanished, and peaks corresponding to smaller molecules, such as m/z = 98 (N′-cyano-N-methyl acetamidine), m/z = 128, and m/z = 158 (6-Chloronicotinic acid), were detected (Cruz-Alcalde et al. 2017). This indicates that ACE was successfully mineralized and demonstrates the high photocatalytic efficiency of TiO_2-doped ZnO.

Comparison with other photocatalytic findings on ACE degradation

Table 2 summarizes recent photocatalytic studies on ACE degradation using different catalysts and irradiation sources. Overall, the literature indicates that TiO_2-based systems under UVA or UV-C commonly yield moderate removal efficiencies, often requiring long reaction times or higher initial ACE concentrations. ZnO and ZnO-based composites, particularly those modified with graphene oxide or noble metals, demonstrate significantly enhanced activity under visible light or solar irradiation, in some cases achieving complete degradation within shorter treatment periods. Compared to these findings, the present study shows that ZnO-based catalysts under UV-C irradiation can achieve complete ACE removal rapidly at low pollutant concentrations without

Table 2 Photocatalytic degradation performance of ACE using various photocatalysts and light sources reported in the literature

Photocatalyst	Light Source	Initial Conc. (C_0) mg/L	pH	Catalyst Dosage	Time (min)	Removal Efficiency (%) and Analytical Method	Reference
TiO_2 (Degussa P-25)	UVA (400–320 nm)	500	5.0	-	420	> %90 (HPLC/DAD, UV spectrophotometry)	(Guzsvány et al. 2009)
TiO_2 (Degussa P-25)	UV (366 nm)	2000	~5.2–5.8	2.0 mg/mL	300	100% (HPLC/DAD)	(Guzsvány et al. 2012)
UV-C pretreated TiO_2	UV-A (365 nm)	10	6.5	160 cm^2	240	%56 (HPLC–UV)	(Zelić et al. 2022)
Perlite-supported TiO_2 catalyst	UVA-LED (365 nm)	10	6.5	-	240	%48.49 (HPLC)	(Kosar et al. 2023)
UV-C pretreated TiO_2 P25	UV-A lamp	2	8	60 mg/0.6 dm^3	120	~%50 (HPLC)	(Licht et al. 2023)
ZnO	Visible light	15	-	0.2 g/L	300	~%40 Gas Chromatography (GC)	(Miyashiro and Hamoudi 2022a)
N-GO-ZnO* and Pd-GO-ZnO** composites	Visible light	15	-	0.2 g/L	180	% 100 (GC)	(Miyashiro and Hamoudi 2022b)
ZnO	Solar irradiation	0.1	~7.1	0.2 g/L	120	%85 (HPLC)	(Fenoll et al. 2015)
TiO_2	Solar irradiation	0.1	~7.1	0.2 g/L	120	%30 (HPLC)	(Fenoll et al. 2015)
ZnO	UV-C	5	6.2	0.1 g/L	120	%79 (UV–Vis); %100 (HPLC)	This study
TiO_2-doped ZnO	UV-C	5	6.2	0.1 g/L	120	%71 (UV–Vis); %100 (HPLC)	This study

*nitrogen-doped graphene oxide zinc oxide; ** palladium-graphene oxide zinc oxide

additives, highlighting their practical potential for efficient and scalable water treatment applications.

Conclusion

In this study, the efficiency of ZnO and TiO_2-doped ZnO photocatalysts for the photocatalytic removal of ACE from aqueous solutions was investigated. In experiments conducted under UV-C light, ZnO exhibited the highest performance with a removal efficiency of 79%, while TiO_2-doped ZnO achieved a removal efficiency of 71%. Kinetic analyses revealed that the degradation rate of ACE followed a pseudo-first-order kinetic model, and ZnO had a higher rate constant. HPLC analyses confirmed that ACE was completely removed (100%) after a reaction time of 120 min; however, due to the presence of intermediate products, UV spectrophotometer analyses showed removal efficiencies of 79% for ZnO and 71% for TiO_2-doped ZnO. It was determined that ZnO exhibited higher photocatalytic activity compared to TiO_2-doped ZnO and was more effective in the rapid oxidation and degradation of ACE. ZnO's ability to generate more photoexcited electron–hole pairs than TiO_2-doped ZnO enhanced its photocatalytic performance. The intermediate products formed during the photocatalytic process were identified using LC–MS/MS, and ACE was transformed into smaller compounds such as hydroxylated derivatives, demethylated fragments, nitrile-containing intermediates, and low-molecular-weight carboxylic acids (e.g., formic and acetic acids) through mechanisms such as C–N bond cleavage, hydroxylation, demethylation, and ring opening. Future studies should include a more detailed toxicological evaluation of these intermediates to better assess the environmental risks of the process.

Future studies could investigate the modification of ZnO and TiO_2 with different additives to enhance the efficiency of the photocatalytic process. In particular, methods that improve photocatalytic activity under visible light are important for energy savings and broader application areas. Additionally, a more detailed examination of the toxicological effects of intermediate products is critical for evaluating

the environmental impacts and potential risks of the process. Developing nano-structures with an expanded surface area for ZnO and exploring ways to increase the reusability of photocatalysts could offer new perspectives for sustainable water treatment technologies. For the industrial application of photocatalytic processes, in addition to scaling-up studies, innovative reactor designs that improve energy efficiency should also be examined.

Supplementary Information The online version contains supplementary material available at https://doi.org/10.1007/s13762-025-06984-3.

Acknowledgements This study was produced from the Master's thesis titled *"Degradation of the Neonicotinoid-containing pesticide (Acetamiprid) using different catalysts by photocatalytic method and investigation of kinetic parameters"* by Esma Sebile Eroğlu, conducted under the supervision of Gökçe Didar Değermenci and co-supervision of Muhammed Bora Akın.

Author contributions Esma Sebile Eroğlu: Investigation, Data curation. Muhammed Bora Akın: Methodology, Visualization, Investigation, Resources, Writing—Original Draft, Writing—Review & Editing. Gökçe Didar Değermenci: Investigation, Methodology, Conceptualization, Writing—Original Draft, Writing—Review & Editing, Supervision.

Funding No funds, grants, or other support were received.

Data availability The datasets used and/or analysed during the current study available from the corresponding author on reasonable request.

Declarations

Conflict of interest The authors declare that they have no conflict of interest.

Ethical approval The authors confirm that this study was conducted in accordance with all applicable ethical guidelines, ensuring the ethical sourcing of experimental materials, the safety of the experimental procedures, and the minimization of environmental impact.

References

Ahmad T, Pandey V, Saddam Husain M et al (2022) Structural and spectroscopic analysis of pure phase hexagonal wurtzite ZnO nanoparticles synthesized by sol-gel. Mater Today Proc 49:1694–1697. https://doi.org/10.1016/j.matpr.2021.07.456

Ahmed SN, Haider W (2018) Heterogeneous photocatalysis and its potential applications in water and wastewater treatment: a review. Nanotechnology 29:342001. https://doi.org/10.1088/1361-6528/aac6ea

Akhter P, Nawaz S, Shafiq I et al (2023) Efficient visible light assisted photocatalysis using ZnO/TiO_2 nanocomposites. Mol Catal 535:112896. https://doi.org/10.1016/j.mcat.2022.112896

Akin B, Oner M (2012) Aqueous pathways for formation of zinc oxide particles in the presence of carboxymethyl inulin. Res Chem Intermed 38:1511–1525. https://doi.org/10.1007/s11164-011-0481-x

Al-Gaashani R, Radiman S, Daud AR et al (2013) XPS and optical studies of different morphologies of ZnO nanostructures prepared by microwave methods. Ceram Int 39:2283–2292. https://doi.org/10.1016/j.ceramint.2012.08.075

AlMohamadi H, Awad SA, Sharma AK et al (2024) Photocatalytic activity of metal- and non-metal-anchored ZnO and TiO_2 nanocatalysts for advanced photocatalysis: comparative study. Catalysts 14:420. https://doi.org/10.3390/catal14070420

Anil K, Surenjan A (2024) Green synthesis, characterisation, and performance evaluation of ZnO/TiO_2 nanocomposite for cationic and anionic dye removal from aqueous solutions under solar irradiation. Water Pract Technol 19:824–838. https://doi.org/10.2166/wpt.2024.022

Asikuzun E, Ozturk O (2018) Theoretical and experimental approaches to measuring mechanical properties of $Zn_{1-x}Co_xO$ binary tetrahedral bulk semiconductors. J Mater Sci Mater Electron 29:7971–7978. https://doi.org/10.1007/s10854-018-8800-2

Asikuzun E, Ozturk O (2019) Comparison of theoretical and experimental microhardness of tetrahedral binary $Zn_{1-x}Er_xO$ semiconductor polycrystalline nanoparticles. Ceram Int 45:4176–4183. https://doi.org/10.1016/j.ceramint.2018.11.086

Aslan Ş, İçli N (2022) Detection of organochlorine pesticides residues in garlic and evaluation of health risks. Turkish J Agricul Natural Sci 9:69–76

Avila R, García-Vara M, López-García E et al (2022) Evaluation of an outdoor pilot-scale tubular photobioreactor for removal of selected pesticides from water. Sci Total Environ 804:150040. https://doi.org/10.1016/j.scitotenv.2021.150040

Baruah S, Dutta J (2009) Hydrothermal growth of ZnO nanostructures. Sci Technol Adv Mater 10:18. https://doi.org/10.1088/1468-6996/10/1/013001

Bass C, Denholm I, Williamson MS, Nauen R (2015) The global status of insect resistance to neonicotinoid insecticides. Pestic Biochem Physiol 121:78–87. https://doi.org/10.1016/j.pestbp.2015.04.004

Beltrán-Flores E, Blánquez P, Gorito AM et al (2024) Combining fungal bioremediation and ozonation for rinse wastewater treatment. Sci Total Environ 912:169198. https://doi.org/10.1016/j.scitotenv.2023.169198

Benhalima T, Mokhtari M, Ferfera-Harrar H (2024) Synergistic adsorption/photodegradation effect for effective removal of crystal violet dye and acetamiprid pesticide using Fe^{3+} cross-linked ternary carboxymethyl cellulose/polyaniline/TiO_2 photocomposites. J Water Process Eng 57:104670. https://doi.org/10.1016/j.jwpe.2023.104670

Berberidou C, Kitsiou V, Karahanidou S et al (2016) Photocatalytic degradation of the herbicide clopyralid: kinetics, degradation pathways and ecotoxicity evaluation. J Chem Technol Biotechnol 91:2510–2518. https://doi.org/10.1002/jctb.4848

Carra I, Sirtori C, Ponce-Robles L et al (2015) Degradation and monitoring of acetamiprid, thiabendazole and their transformation products in an agro-food industry effluent during solar photo-Fenton treatment in a raceway pond reactor. Chemosphere 130:73–81. https://doi.org/10.1016/j.chemosphere.2015.03.001

Chen L, Cai T, Cheng C et al (2018) Degradation of acetamiprid in UV/H_2O_2 and UV/persulfate systems: a comparative study. Chem Eng J 351:1137–1146. https://doi.org/10.1016/j.cej.2018.06.107

Cruz-Alcalde A, Sans C, Esplugas S (2017) Priority pesticides abatement by advanced water technologies: the case of acetamiprid removal by ozonation. Sci Total Environ 599–600:1454–1461. https://doi.org/10.1016/j.scitotenv.2017.05.065

Cui S, Lv J, Hough R et al (2024) Recent advances and prospects of neonicotinoid insecticides removal from aquatic environments using biochar: adsorption and degradation mechanisms. Sci Total Environ 939:173509. https://doi.org/10.1016/j.scitotenv.2024.173509

Darvishi Cheshmeh Soltani R, Khataee AR, Mashayekhi M (2016) Photocatalytic degradation of a textile dye in aqueous phase over

ZnO nanoparticles embedded in biosilica nanobiostructure. Desalin Water Treat 57:13494–13504. https://doi.org/10.1080/19443994.2015.1058193

Ekthammathat N, Thongtem T, Phuruangrat A, Thongtem S (2013) Growth of hexagonal prism ZnO nanorods on Zn substrates by hydrothermal method and their photoluminescence. Ceram Int 39:S501–S505. https://doi.org/10.1016/j.ceramint.2012.10.122

Elbert A, Haas M, Springer B et al (2008) Applied aspects of neonicotinoid uses in crop protection. Pest Manag Sci 64:1099–1105. https://doi.org/10.1002/ps.1616

Esfandian H, Rostamnejad Cherati M, Khatirian M (2024) Electrochemical behavior and photocatalytic performance of chlorpyrifos pesticide decontamination using Ni-doped ZnO-TiO_2 nanocomposite. Inorg Chem Commun 159:111750. https://doi.org/10.1016/j.inoche.2023.111750

Fenoll J, Garrido I, Hellín P et al (2015) Photodegradation of neonicotinoid insecticides in water by semiconductor oxides. Environ Sci Pollut Res 22:15055–15066. https://doi.org/10.1007/s11356-015-4721-2

Ganie AS, Bano S, Khan N et al (2021) Nanoremediation technologies for sustainable remediation of contaminated environments: recent advances and challenges. Chemosphere 275:130065. https://doi.org/10.1016/j.chemosphere.2021.130065

Garber K, Steeger T (2008) Problem Formulation for the Environmental Fate and Ecological Risk, Endangered Species and Drinking Water Assessments in Support of the Registration Review of Diazinon. Washington, DC

Gonçalves RA, Toledo RP, Joshi N, Berengue OM (2021) Green synthesis and applications of ZnO and TiO_2 nanostructures. Molecules 26:2236. https://doi.org/10.3390/molecules26082236

Guzsvány VJ, Csanádi JJ, Lazić SD, Gaál FF (2009) Photocatalytic degradation of the insecticide acetamiprid on TiO_2 catalyst. J Braz Chem Soc 20:152–159. https://doi.org/10.1590/s0103-50532009000100023

Guzsvány V, Rajić L, Jović B et al (2012) Spectroscopic monitoring of photocatalytic degradation of the insecticide acetamiprid and its degradation product 6-chloronicotinic acid on TiO_2 catalyst. J Environ Sci Health A Tox Hazard Subst Environ Eng 47:1919–1929. https://doi.org/10.1080/03601234.2012.676452

Habib MA, Shahadat MT, Bahadur NM et al (2013) Synthesis and characterization of ZnO-TiO_2 nanocomposites and their application as photocatalysts. Int Nano Lett 3:5. https://doi.org/10.1186/2228-5326-3-5

Hamdani K, Belhousse S, Tighilt FZ et al (2022) Impedance investigation of TiO_2 nanotubes/nanoparticles-based dye-sensitized solar cells. J Mater Res 37:500–508. https://doi.org/10.1557/s43578-021-00464-3

Hashemi Monfared A, Jamshidi M (2019) Synthesis of polyaniline/titanium dioxide nanocomposite (PAni/TiO_2) and its application as photocatalyst in acrylic pseudo paint for benzene removal under UV/VIS lights. Prog Org Coat 136:105257. https://doi.org/10.1016/j.porgcoat.2019.105257

Hashimoto K, Irie H, Fujishima A (2005) TiO_2 photocatalysis: a historical overview and future prospects. Jpn J Appl Phys 44:8269–8285. https://doi.org/10.1143/JJAP.44.8269

Ibrahim MM, Mezni A, Alsawat M et al (2020) Crystalline ZnO and ZnO/TiO_2 nanoparticles derived from *tert*-butyl N-(2 mercaptoethyl)carbamatozinc(II) chelate: electrocatalytic studies for H_2 generation in alkaline electrolytes. Int J Energy Res 44:6725–6744. https://doi.org/10.1002/er.5410

James KL, Randall NP, Walters KFA et al (2016) Evidence for the effects of neonicotinoids used in arable crop production on non-target organisms and concentrations of residues in relevant matrices: a systematic map protocol. Environ Evid 5:22. https://doi.org/10.1186/s13750-016-0072-9

Kosar V, Križanac AM, Zelić IE et al (2023) Photocatalytic degradation of neonicotinoid insecticides over perlite-supported TiO_2. Processes 11:2588. https://doi.org/10.3390/pr11092588

Kosmulski M (2002) The significance of the difference in the point of zero charge between rutile and anatase. Adv Colloid Interface Sci 99:255–264. https://doi.org/10.1016/S0001-8686(02)00080-5

Kosmulski M (2020) The pH dependent surface charging and points of zero charge. VIII. Update. Adv Colloid Interface Sci 275:102064. https://doi.org/10.1016/j.cis.2019.102064

Licht K, Kosar V, Tomašić V, Duplančić M (2023) Removal of the neonicotinoid insecticide acetamiprid from wastewater using heterogeneous photocatalysis. Environ Technol 44:1125–1134. https://doi.org/10.1080/09593330.2021.1994656

Lima ÉC, Adebayo MA, Machado FM (2015) Kinetic and equilibrium models of adsorption. Carbon Nanomaterials as Adsorbents for Environmental and Biological Applications. Springer, Cham, pp 33–69

Lin J, Wang L (2009) Comparison between linear and non-linear forms of pseudo-first-order and pseudo-second-order adsorption kinetic models for the removal of methylene blue by activated carbon. Front Environ Sci Eng China 3:320–324. https://doi.org/10.1007/s11783-009-0030-7

Liu J, Gao Y, Zhang Z et al (2023) Photocatalytic activity of TiO_2-ZnO/g-C_3N_4 nanocomposites for methylene orange and Rhodamine B dyes removal from water and photocatalytic hydrogen generation. Chemosphere 339:139426. https://doi.org/10.1016/j.chemosphere.2023.139426

Liu Z, Lin J, Xu Z et al (2024) Highly effective Fe-doped nano titanium oxide for removal of acetamiprid and atrazine under simulated sunlight irradiation. Agronomy 14:461. https://doi.org/10.3390/agronomy14030461

Mazabuel-Collazos A, Rodríguez-Páez JE (2018) Chemical synthesis and characterization of ZnO-TiO_2 semiconductor nanocomposites: tentative mechanism of particle formation. J Inorg Organomet Polym Mater 28:1739–1752. https://doi.org/10.1007/s10904-018-0827-6

Miyashiro CS, Hamoudi S (2022a) Aqueous acetamiprid degradation using combined ultrasonication and photocatalysis under visible light. Water Air Soil Pollut 233:401. https://doi.org/10.1007/s11270-022-05867-4

Miyashiro CS, Hamoudi S (2022b) Palladium and graphene oxide doped ZnO for aqueous acetamiprid degradation under visible light. Catalysts 12:709. https://doi.org/10.3390/catal12070709

Mohsenzadeh M, Mirbagheri SA, Sabbaghi S (2019) Degradation of 1,2-dichloroethane by photocatalysis using immobilized PAni-TiO_2 nano-photocatalyst. Environ Sci Pollut Res 26:31328–31343. https://doi.org/10.1007/s11356-019-06240-5

Morrissey CA, Mineau P, Devries JH et al (2015) Neonicotinoid contamination of global surface waters and associated risk to aquatic invertebrates: a review. Environ Int 74:291–303. https://doi.org/10.1016/j.envint.2014.10.024

Murugesan A, Loganathan M, Senthil Kumar P, Vo DVN (2021) Cobalt and nickel oxides supported activated carbon as an effective photocatalysts for the degradation methylene blue dye from aquatic environment. Sustain Chem Pharm 21:100406. https://doi.org/10.1016/j.scp.2021.100406

Nawaz R, Ullah H, Ghanim AAJ et al (2023) Green synthesis of ZnO and black TiO_2 materials and their application in photodegradation of organic pollutants. ACS Omega 8:36076–36087. https://doi.org/10.1021/acsomega.3c04229

Nosaka Y, Nosaka AY (2017) Generation and detection of reactive oxygen species in photocatalysis. Chem Rev 117:11302–11336. https://doi.org/10.1021/acs.chemrev.7b00161

O'Neill S, Robertson JMC, Héquet V et al (2023) Comparison of Titanium Dioxide and Zinc Oxide Photocatalysts for the Inactivation of Escherichia coli in Water Using Slurry and

Rotating-Disk Photocatalytic Reactors. Ind Eng Chem Res 62:18952–18959. https://doi.org/10.1021/acs.iecr.3c00508
Pan H, Zhang Y, Hu Y, Xie H (2020) Effect of cobalt doping on optical, magnetic and photocatalytic properties of ZnO nanoparticles. Optik (Stuttg) 208:164560. https://doi.org/10.1016/j.ijleo.2020.164560
Papitha R, Hadkar V, Sishu NK et al (2024) Green synthesis of CuO/TiO_2 and ZnO/TiO_2 nanocomposites using *Parkia timoriana* bark extract: enhanced antioxidant and antidiabetic activities for biomedical applications. Ceram Int 50:39109–39121. https://doi.org/10.1016/j.ceramint.2024.07.277
Pelaez M, Nolan NT, Pillai SC et al (2012) A review on the visible light active titanium dioxide photocatalysts for environmental applications. Appl Catal B 125:331–349. https://doi.org/10.1016/j.apcatb.2012.05.036
Phogat A, Singh J, Kumar V, Malik V (2022) Toxicity of the acetamiprid insecticide for mammals: a review. Environ Chem Lett 20:1453–1478. https://doi.org/10.1007/s10311-021-01353-1
Popadić D, Gavrilov N, Krstić J et al (2023) Spectral evidence of acetamiprid's thermal degradation products and mechanism. Spectrochim Acta Part A Mol Biomol Spectrosc 301:122987. https://doi.org/10.1016/j.saa.2023.122987
Prabhu A, Meenu PC, Roy S (2024) Creation of a facile heterojunction in Co/ZnO-TiO_2 for the photocatalytic degradation of alizarin S. New J Chem 48:10552–10562. https://doi.org/10.1039/d4nj00407h
Premalatha N, Rex P (2024) A comprehensive review on photocatalytic degradation of organophosphorus pesticide using ZnO coupled photocatalysts. Desalin Water Treat 320:100753. https://doi.org/10.1016/j.dwt.2024.100753
Qin R, Meng F, Khan MW et al (2019) Fabrication and enhanced photocatalytic property of TiO_2-ZnO composite photocatalysts. Mater Lett 240:84–87. https://doi.org/10.1016/j.matlet.2018.12.139
Sathishkumar P, Mangalaraja RV, Rozas O et al (2016) Sonophotocatalytic mineralization of Norflurazon in aqueous environment. Chemosphere 146:216–225. https://doi.org/10.1016/j.chemosphere.2015.12.011
Sawunyama L, Oyewo O, Onwudiwe DC, Makgato SS (2023) Photocatalytic degradation of tetracycline using surface defective black TiO_2-ZnO heterojunction photocatalyst under visible light. Heliyon 9:e21423. https://doi.org/10.1016/j.heliyon.2023.e21423
Sayury Miyashiro C, Hamoudi S (2021) Visible light driven photocatalytic degradation of aqueous acetamiprid over nitrogen and graphene oxide doped ZnO composites. RSC Adv 11:22508–22516. https://doi.org/10.1039/d1ra02098f
Scarano D, Bertarione S, Cesano F et al (2006) Plate-like zinc oxide microcrystals: synthesis and characterization of a material active toward hydrogen adsorption. Catal Today 116:433–438. https://doi.org/10.1016/j.cattod.2006.05.062
Sellaoui L, Gómez-Avilés A, Dhaouadi F et al (2023) Adsorption of emerging pollutants on lignin-based activated carbon: analysis of adsorption mechanism via characterization, kinetics and equilibrium studies. Chem Eng J 452:139399. https://doi.org/10.1016/j.cej.2022.139399
Serrano E, Munoz M, de Pedro ZM, Casas JA (2020) Fast oxidation of the neonicotinoid pesticides listed in the EU decision 2018/840 from aqueous solutions. Sep Purif Technol 235:116168. https://doi.org/10.1016/j.seppur.2019.116168
Shathy RA, Fahim SA, Sarker M et al (2022) Natural sunlight driven photocatalytic removal of toxic textile dyes in water using B-doped ZnO/TiO_2 nanocomposites. Catalysts 12:308. https://doi.org/10.3390/catal12030308
Simonin JP (2016) On the comparison of pseudo-first order and pseudo-second order rate laws in the modeling of adsorption kinetics. Chem Eng J 300:254–263. https://doi.org/10.1016/j.cej.2016.04.079
Soriano-Molina P, García Sánchez JL, Malato S et al (2018) Effect of volumetric rate of photon absorption on the kinetics of micropollutant removal by solar photo-Fenton with Fe^{3+}-EDDS at neutral pH. Chem Eng J 331:84–92. https://doi.org/10.1016/j.cej.2017.08.096
Tahoun B, Mansour S, Tony M, Farag S (2022) Development and characterization of conjugated polyaniline/Co-doped ZnO nanocomposites for enhanced dye oxidation from wastewater. Eng Res J 45:101. https://doi.org/10.21608/erjm.2022.104420.1120
Taie M, Fadaei A, Sadeghi M et al (2021) Comparison of the efficiency of ultraviolet/zinc oxide (UV/ZnO) and ozone/zinc oxide (O_3/ZnO) techniques as advanced oxidation processes in the removal of trimethoprim from aqueous solutions. Int J Chem Eng 2021:9640918. https://doi.org/10.1155/2021/9640918
Tran HN, You SJ, Hosseini-Bandegharaei A, Chao HP (2017) Mistakes and inconsistencies regarding adsorption of contaminants from aqueous solutions: a critical review. Water Res 120:88–116. https://doi.org/10.1016/j.watres.2017.04.014
Tsegay G, Lartey-Young G, Sibhat M et al (2024) An integrated approach to assess human health risk of neonicotinoid insecticides in surface water of the Yangtze River Basin, China. J Hazard Mater 469:133915. https://doi.org/10.1016/j.jhazmat.2024.133915
Turkten N, Bekbolet M (2020) Photocatalytic performance of titanium dioxide and zinc oxide binary system on degradation of humic matter. J Photochem Photobiol A Chem 401:112748. https://doi.org/10.1016/j.jphotochem.2020.112748
Vasanth Kumar K, Porkodi K, Selvaganapathi A (2007) Constrain in solving Langmuir-Hinshelwood kinetic expression for the photocatalytic degradation of Auramine O aqueous solutions by ZnO catalyst. Dye Pigment 75:246–249. https://doi.org/10.1016/j.dyepig.2006.05.035
Vidya C, Manjunatha C, Sudeep M et al (2020) Photo-assisted mineralisation of titan yellow dye using ZnO nanorods synthesised via environmental benign route. SN Appl Sci 2:743. https://doi.org/10.1007/s42452-020-2537-2
Viñes F, Iglesias-Juez A, Illas F, Fernández-García M (2014) Hydroxyl identification on ZnO by infrared spectroscopies: theory and experiments. J Phys Chem C 118:1492–1505. https://doi.org/10.1021/jp407021v
Wang H, Huang Y, Shen C et al (2016) Co-transport of pesticide acetamiprid and silica nanoparticles in biochar-amended sand porous media. J Environ Qual 45:1749–1759. https://doi.org/10.2134/jeq2016.02.0073
Wang F, Liu Y, Cao M et al (2023) Mechanisms of ZnO nanoparticles enhancing phototransformation of biologically derived organic phosphorus in aquatic environments. Environ Sci Technol 57:3691–3702. https://doi.org/10.1021/acs.est.3c00704
Wu K, Dong X, Zhu J et al (2018) Designing biomimetic porous celery: TiO_2/ZnO nanocomposite for enhanced CO_2 photoreduction. J Mater Sci 53:11595–11606. https://doi.org/10.1007/s10853-018-2397-y
Yamada T, Takahashi H, Hatano R (1999) A Novel Insecticide, Acetamiprid. In: Nicotinoid Insecticides and the Nicotinic Acetylcholine Receptor. Springer, Tokyo, pp 149–176. https://doi.org/10.1007/978-4-431-67933-2_7
Yang X, Zhao R, Zhan H et al (2024) Modified titanium dioxide-based photocatalysts for water treatment: mini review. Environmental Functional Materials 3:1–12. https://doi.org/10.1016/j.efmat.2024.07.002
Yusuff AS, Popoola LT, Gbadamosi AO, Igbafe AI (2024) Coal fly ash-supported ZnO-promoted TiO_2 towards UV photocatalytic degradation of anthraquinone dye: parametric optimization, kinetics and mechanism studies. Mater Today Commun 38:107999. https://doi.org/10.1016/j.mtcomm.2023.107999

Zbiljić J, Guzsvány V, Vajdle O et al (2015) Determination of H_2O_2 by MnO_2 modified screen printed carbon electrode during Fenton and visible light-assisted photo-Fenton based removal of acetamiprid from water. J Electroanal Chem 755:77–86. https://doi.org/10.1016/j.jelechem.2015.07.027

Zelić IE, Povijač K, Gilja V et al (2022) Photocatalytic degradation of acetamiprid in a rotating photoreactor—determination of reactive species. Catal Commun 169:106474. https://doi.org/10.1016/j.catcom.2022.106474

Zhang X, Cao Y, Cao J et al (2024a) Neonicotinoid insecticides in waters of the northern Jiangsu segment of the Beijing-Hangzhou Grand Canal: environmental and health implications. Sci Total Environ 923:171455. https://doi.org/10.1016/j.scitotenv.2024.171455

Zhang Y, Bo X, Zhu T et al (2024b) Synthesis of TiO_2-ZnO n-n heterojunction with excellent visible light-driven photodegradation of tetracycline. Nanomaterials 14:1802. https://doi.org/10.3390/nano14221802